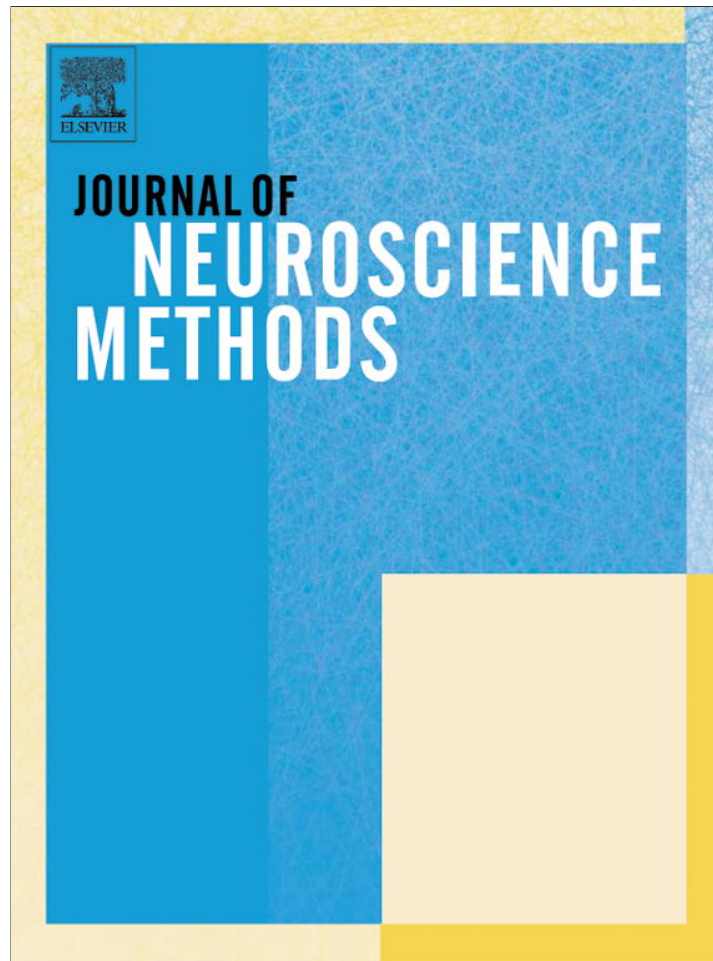


Provided for non-commercial research and education use.  
Not for reproduction, distribution or commercial use.



(This is a sample cover image for this issue. The actual cover is not yet available at this time.)

**This article appeared in a journal published by Elsevier. The attached copy is furnished to the author for internal non-commercial research and education use, including for instruction at the authors institution and sharing with colleagues.**

**Other uses, including reproduction and distribution, or selling or licensing copies, or posting to personal, institutional or third party websites are prohibited.**

**In most cases authors are permitted to post their version of the article (e.g. in Word or Tex form) to their personal website or institutional repository. Authors requiring further information regarding Elsevier's archiving and manuscript policies are encouraged to visit:**

**<http://www.elsevier.com/copyright>**



Contents lists available at SciVerse ScienceDirect

## Journal of Neuroscience Methods

journal homepage: [www.elsevier.com/locate/jneumeth](http://www.elsevier.com/locate/jneumeth)

Basic Neuroscience

## Adaptive time-varying detrended fluctuation analysis

Luc Berthouze<sup>a,b,\*</sup>, Simon F. Farmer<sup>c</sup><sup>a</sup> Centre for Computational Neuroscience and Robotics, University of Sussex, UK<sup>b</sup> Institute of Child Health, UCL, UK<sup>c</sup> Institute of Neurology, UCL, UK

## HIGHLIGHTS

- ▶ DFA is often used to estimate the scaling exponent of neurophysiological signals.
- ▶ We extend DFA to characterise potentially changing scaling exponents.
- ▶ We validate the method using surrogate data with time-varying scaling exponents.
- ▶ We systematically examine the dependence of the method on its free parameters.
- ▶ We demonstrate the applicability of the method to neurophysiological signals.

## ARTICLE INFO

## Article history:

Received 21 October 2011

Received in revised form 24 May 2012

Accepted 28 May 2012

## Keywords:

Long-range temporal correlations

Long-range dependence

Scaling exponent

Neurophysiological time series

EEG

Detrended fluctuation analysis

Kalman filter

Non stationarity

## ABSTRACT

Detrended fluctuation analysis (DFA) is a technique commonly used to assess and quantify the presence of long-range temporal correlations (LRTCs) in neurophysiological time series. Convergence of the method is asymptotic only and therefore its application assumes a constant scaling exponent. However, most neurophysiological data are likely to involve either spontaneous or experimentally induced scaling exponent changes. We present a novel extension of the DFA method that permits the characterisation of time-varying scaling exponents. The effectiveness of the methodology in recovering known changes in scaling exponents is demonstrated through its application to synthetic data. The dependence of the method on its free parameters is systematically explored. Finally, application of the methodology to neurophysiological data demonstrates that it provides experimenters with a way to identify previously un-recognised changes in the scaling exponent in the data. We suggest that this methodology will make it possible to go beyond a simple demonstration of the presence of scaling to an appreciation of how it may vary in response to either intrinsic changes or experimental perturbations.

© 2012 Elsevier B.V. All rights reserved.

## 1. Introduction

Neurophysiological processes are interaction dominated such that the operation of one component of the system closely depends on the state of another component. In contrast to systems dominated by additive and subtractive interactions, which produce distributions characterised by Gaussian statistics, neuronal activity is characterised by multiplicative interactions that can produce heavy-tailed distributions including power law distributions (Kello et al., 2010).

It has now been established that many neurophysiological signals show power law distributions of their autocovariance function,

i.e., they exhibit long-range temporal correlations (LRTCs). These LRTCs have been observed in fluctuations of amplitudes (e.g., Linkenkaer-Hansen et al., 2001, 2004; Nikulin and Brismar, 2005; Berthouze et al., 2010) and inter-event intervals (Hartley et al., 2012). The detection and characterisation of LRTCs in neurophysiological data has received great attention in part due to the fact that LRTCs are a (necessary, but not sufficient) signature of critical systems. The idea that the brain may be operating in a critical regime is very attractive (Chialvo, 2010) because critical systems have been shown to maximise their dynamic range of processing (Kinouchi and Copelli, 2006; Shew et al., 2009; Buckley and Nowotny, 2011), and implement balanced activity (Benayoun et al., 2010; Magnasco et al., 2009; Meisel and Gross, 2009). In their seminal work, Linkenkaer-Hansen et al. (2001) interpreted the presence of LRTCs in the fluctuations of EEG and MEG amplitude oscillations within the framework of criticality in which once LRTCs are established, the scaling exponent would be expected to be constant throughout a normal resting state neurophysiological record. From the perspective of criticality (in its physics sense of the term),

\* Corresponding author at: Centre for Computational Neuroscience and Robotics, University of Sussex, Falmer BN1 9QH, UK. Tel.: +44 1273 877206; fax: +44 1273 877873.

E-mail addresses: [L.Berthouze@sussex.ac.uk](mailto:L.Berthouze@sussex.ac.uk) (L. Berthouze), [S.Farmer@ucl.ac.uk](mailto:S.Farmer@ucl.ac.uk) (S.F. Farmer).

such an assumption may be justified. However, there is an alternative view which is that heavy-tailed distributions (including power laws) could also be observed as the result of the superposition of processes with distinct time scales (Wagenmakers et al., 2004), or as a result of measurements (Touboul and Destexhe, 2010). In this view, the validity of the assumption that the scaling exponent is constant throughout a neurophysiological recording should be firmly established because the overall organisation of these different time scales may no longer result from a global order parameter. We suggest that any exponent estimation method should be agnostic to the origin of the LRTCs and instead focus on providing a robust estimation of exponent magnitude over small enough time scales within which exponent magnitude fluctuations if present can be observed.

Furthermore, LRTCs in neurophysiological time series have been characterised using estimates of the Hurst exponent which quantifies the slope of the auto-covariance function of the signal, with exponents in the interval (0.5,1] denoting the presence of LRTCs. These estimates can be obtained using several methodologies, see Taqqu and Teverovsky (1995) and Serinaldi (2010) for comprehensive comparative reviews of methods operating in both time and frequency domains, including detrended fluctuation analysis (DFA, Peng et al., 1994). These methodologies estimate the statistical properties of the data under the implicit assumption of constancy of the scaling properties of the signal. Therefore, they are by definition insensitive to any within time series change in the exponent magnitude that characterises LRTCs.

In the case of DFA, which has been extensively used in the neurophysiology literature, if the changes are small enough, the scaling property of the detrended fluctuations can be maintained (based on the  $R^2$  value of the linear regression being greater than a given threshold, typically 0.95) and therefore the method, as commonly implemented in published reports, will return valid exponents without any indication that the assumption of scaling exponent constancy has been violated. Only close inspection or a more robust test of the distribution of the fluctuations in the log–log scale could provide an indication of superposition of processes (Chen et al., 2002; Hu et al., 2001).

To date, there have been a few attempts to track changes in the scaling parameter and these attempts have relied on a rolling implementation of standard DFA methodologies over moving windows (e.g., Alvarez-Ramirez et al., 2008; Peña et al., 2009; Yue et al., 2010). This approach does not involve optimal filtering and has not been validated against time series in which the magnitude of the scaling exponent is systematically manipulated within the record. Further, this approach when applied to non-physiological time-series has been shown to lead to erratic behaviour in the estimates of the scaling exponent (Alvarez-Ramirez et al., 2008; Peña et al., 2009).

Here, we present a novel extension of the detrended fluctuation analysis method (adaptive time-varying detrended fluctuation analysis – ATvDFA) which permits the robust characterisation of time-varying scaling parameters. We systematically compare the ATvDFA method with a moving windows DFA using synthetic data and demonstrate its applicability within 3 different types of neurophysiological time series.

## 2. Material and methods

### 2.1. Method formulation

The core component of the method is detrended fluctuation analysis, and it is briefly summarised here. We assume a bounded

time series  $x(i)$ , where  $i = \{1, \dots, N\}$ , and  $N$  is the length of the signal. First, we construct the integrated signal  $y(i)$  as the cumulated sum:

$$y(i) = \sum_{j=1}^i (x(j) - \bar{x}) \quad (1)$$

We then construct a set of box sizes  $s(k)$  with  $k = \{1, \dots, n\}$  that are equidistant in logarithmic space where  $n$  is suitably large to provide enough resolution in the interval  $[s(1), s(n)]$ , with  $s(1)$  and  $s(n)$  the inner and outer cut-offs, chosen to maximise the range of temporal correlations whilst providing a sufficiently high number of non-overlapping segments for all box size (Peng et al., 1994). For each box size  $s(k)$ , the integrated signal is then split into  $\lfloor N/s(k) \rfloor$  non-overlapping segments, where  $\lfloor x \rfloor$  denotes the largest integer not greater than  $x$ . The signal is then locally detrended by subtracting a polynomial fit  $\hat{y}(i)$ . Finally, for each box size  $s(k)$ , the root mean square fluctuation for the detrended integrated signal is computed:

$$F(s(k)) = \sqrt{\sum_{i=1}^N (y(i) - \hat{y}(i))^2} \quad (2)$$

For signals with long-range temporal correlations, there is a power-law relationship between the root mean square fluctuation  $F(s(k))$  and  $s(k)$ :

$$F(s(k)) \approx s(k)^\alpha \quad (3)$$

where  $\alpha$  is the scaling exponent and is readily obtained by linear regression of the log detrended fluctuations over the log box sizes. The exponent is accepted if the  $R^2$  value is sufficiently high (typically >0.95) and there is no cross-over in the linear scaling of the log detrended fluctuations in relation to the log box sizes (Chen et al., 2002). Convergence of the method is asymptotic only in the limit of  $N$ , the number of samples (Bardet, 2008; Taqqu and Teverovsky, 1995), and therefore the recommended practice is that it should be applied to lengthy time series under the implicit assumption of a constant scaling exponent. However, it has been recently suggested that robust estimates can be obtained even with extremely short time series, especially if the data have genuine long-range correlations (Crevecoeur et al., 2010).

The simplest solution to the problem of detecting changes would be to compute DFA within a moving window (we will refer to this method as mDFA henceforth). Such an approach has been used with non-physiological data previously but leads to considerable statistical variation in the estimates of the scaling exponent (Peña et al., 2009). For short time-series, the application of linear regression of the log fluctuations over the log box size does not lead to a robust estimate of the exponent because of the violation of homoscedasticity, i.e., the fact that the variance in the fluctuations at each box is not identical for all box sizes. Here, we address this problem through the application of a Kalman filter, a data-adaptive filtering procedure, in order to track exponent estimates obtained from overlapping data segments.

A Kalman filter operates over a state-space model, with state and measurement equations given by

$$x_{k+1} = \phi_k x_k + w_k \quad (4)$$

$$z_{k+1} = H_k x_k + v_k \quad (5)$$

where  $x_k$  and  $z_k$  are the state and measurement vectors,  $\phi_k$  is the state transition matrix,  $H_k$  is the state-to-measurement matrix, and  $w_k$  and  $v_k$  are the process and measurement noise sources respectively. Here, we define the state as the parameters of the linear regression of the log detrended fluctuations  $\log F(s(k))_{k=\{1, \dots, m\}}$  over the log box sizes  $\log s(k)_{k=\{1, \dots, m\}}$ . The state vector  $x_k$  is therefore defined as the  $2 \times 1$  column vector  $x_k = [u_1, u_2]$  where  $u_1$  is the

slope (the estimated exponent) of the regression, and  $u_2$  is the intercept. We expect the filter to estimate the local changes in those regression parameters based on our statistical knowledge of the fluctuations. Since the statistics of the regression parameters over each segment are not known, we set the measurement vector  $z_k$  to be the log detrended fluctuations over a single segment because their statistical properties are known for some long-range dependent processes (see Bardet, 2008, for results on a general class of stationary long-range dependent processes).  $z_k$  is therefore given by the  $n \times 1$  column vector  $z_k = [\log F(s(1)), \dots, \log F(s(i)), \dots, \log F(s(n))]$  where  $\log F(s(i))$  is the log transformed root mean squared detrended fluctuation at box size  $s(i)$ . As the state estimates are the parameters of the linear regression of the  $\log F(s(k))_{k=1, \dots, n}$  over the  $\log s(k)_{k=1, \dots, n}$  box sizes, the state-to-measurement matrix  $H_k$  in the case of 1-DFA (linear DFA) is simply given by the constant  $n \times 2$  matrix:

$$H_k = \begin{bmatrix} \log s(1) & 1 \\ \log s(2) & 1 \\ \vdots & \vdots \\ \log s(n) & 1 \end{bmatrix} \quad (6)$$

As we have no reason to assume a systematic change in the state parameters, we set the state-transition matrix  $\phi$  to be the  $2 \times 2$  identity matrix  $I$ . We therefore expect the filter to track any exponent changes through the process noise term  $w_k$  (a  $2 \times 1$  column vector). The process noise term is assumed to be normally distributed with zero mean and ( $2 \times 2$  diagonal) covariance matrix  $Q$ . As in Brittain et al. (2009), this covariance matrix  $Q$  is considered a tracking parameter and is therefore kept constant, the diagonal terms being free parameters of our method. The role of these free parameters will be illustrated in Section 3.1.1 and in the Discussion. Finally, the measurement noise  $r_k$  (a  $n \times 1$  column vector) is also considered to be normally distributed with zero mean and ( $n \times n$  diagonal) covariance matrix  $R_k$ . Here, we propose that robust estimates of this covariance matrix can be obtained by computing the variance of the single-segment log fluctuations over multiple overlapping segments shifted by a small increment. In practice, we used a minimum of 10 measurements between each segment used in the filtering process, e.g., one measurement every 100 ms for an increment of 1 s between estimates. This is possible if one assumes that for very small increments, the scaling exponent will be constant, that is, we assume that changes in scaling exponent (either spontaneous or experimentally induced) occur on a time scale that is much smaller than that of the generators of the intrinsic fluctuations. In such cases, it can be shown (derivation not provided, but trivial using the method of Taqqu and Teverovsky (1995) for fractional Gaussian noise) that the expected value of the difference between exponents of shifted time series is zero.

The Kalman filter algorithm is initialised by

$$x_2^p = x_1, \quad P_2^p = P_1 + Q \quad (7)$$

with  $x_1$  and  $R_1$  the a posteriori estimates of the state and error-covariance matrix at the first segment and  $x_2^p$  and  $P_2^p$  the a priori state and error covariance matrix for the second segment. We initialise  $x_1$  to the regression parameters (slope and intercept) obtained by applying DFA on the first segment.  $P_1 = R_1$  and is computed as per above. Kalman tracking is then performed by using the following update and projection equations for  $k=2, \dots, M$  (Brown and Hwang, 1997).

Update

$$K_k = P_k^p (P_k^p + R)^{-1} \quad (8)$$

$$x_k = x_k^p + K_k (z_k - x_k^p) \quad (9)$$

$$P_k = (I - K_k) P_k^p \quad (10)$$

Projection

$$x_{k+1}^p = x_k \quad (11)$$

$$P_{k+1} = P_k + Q \quad (12)$$

Here, it should be noted that the degree of temporal localisation of the estimate is dependent upon the choice of filter parameters (specifically  $Q$ ) leading to a fundamental trade-off between temporal localisation and consistency (see Sections 3.1.1 and 4). As in Brittain et al. (2009), smoothed estimates can be obtained by employing Kalman equations derived to provide optimal estimates of the smoothed state vector and error-covariance matrix. The full equations are given in Brown and Hwang (1997) and produce exponent estimates that are conditioned on the entire measurement sequence through filtering in the forward direction and then filtering the forward output in a backwards direction.

The methods were implemented as scripts in the Matlab™ environment and build on publicly available code, specifically the DFA implementation (McSharry, 2009) and the EKF/UKF Toolbox for Matlab V1.3 (Hartikainen et al., 2011). The ATvDFA scripts are available from the first author upon request.

## 2.2. Synthetic data

To systematically investigate the tracking capabilities of ATvDFA, time-series were constructed such that their local exponent slowly fluctuated in time, i.e., with the timescale of the fluctuations 3 orders of magnitude lower than that of the sampling frequency. Fractional autoregressive integrated moving average (FARIMA) processes were used. A FARIMA(p,d,q) process  $\{X_t : t = \dots, -1, 0, 1, \dots\}$  is formally defined to be:

$$\Phi(B) \Delta^d X_t = \Theta(B) a_t \quad (13)$$

where

$$\Phi(B) = 1 - \phi_1 B - \phi_2 B^2 - \dots - \phi_p B^p \quad (14)$$

$$\Theta(B) = 1 - \theta_1 B - \theta_2 B^2 - \dots - \theta_q B^q \quad (15)$$

$B$  is the backward-shift operator, i.e.,  $BX_t = X_{t-1}$ ,  $\{a_t\}$  is a white noise,  $p$  and  $q$  are non-negative integers,  $\Delta$  is the differencing operator and  $\Delta^d$  denotes the fractional differencing operator,

$$\Delta^d = (1 - B)d = \sum_{k=0}^{\infty} \binom{d}{k} (-B)^k \quad (16)$$

with  $d \in (-0.5, 0.5)$  and

$$\binom{d}{k} = \frac{\Gamma(d+1)}{\Gamma(k+1)\Gamma(d-k+1)} \quad (17)$$

where  $\Gamma$  denotes the Gamma function. FARIMA processes are the generalisation of standard ARIMA (p,d,q) processes (defined in Box and Jenkins, 1976) where the degree of differencing  $d$  is allowed to take nonintegral values (Hosking, 1981). FARIMA(p,0,q) processes are the usual ARMA(p,q) processes. FARIMA(p,d,q) processes with  $d \in (0, 0.5)$  exhibit long-range dependence. The simple FARIMA(0,d,0) process is similar to the fractional Gaussian noise process used to demonstrate convergence of DFA (Bardet, 2008). The parameter  $d$  relates to the Hurst exponent estimated by DFA through  $H = d + 0.5$ . Here, FARIMA(0,d,0) processes were constructed where  $d$  took the values 0.1271 at  $t=0$  s, 0.1569 at  $t=60$  s, 0.2681 at  $t=70$  s, 0.4018 at  $t=80$  s, 0.4491 at  $t=90$  s, 0.4018 at  $t=150$  s, 0.2681 at  $t=160$  s, 0.1569 at  $t=170$  s, and finally 0.1271 at  $t=180$  s, as shown by the black line in the bottom panel of Fig. 1A (H values shown). All signals had unit variance. The variance of

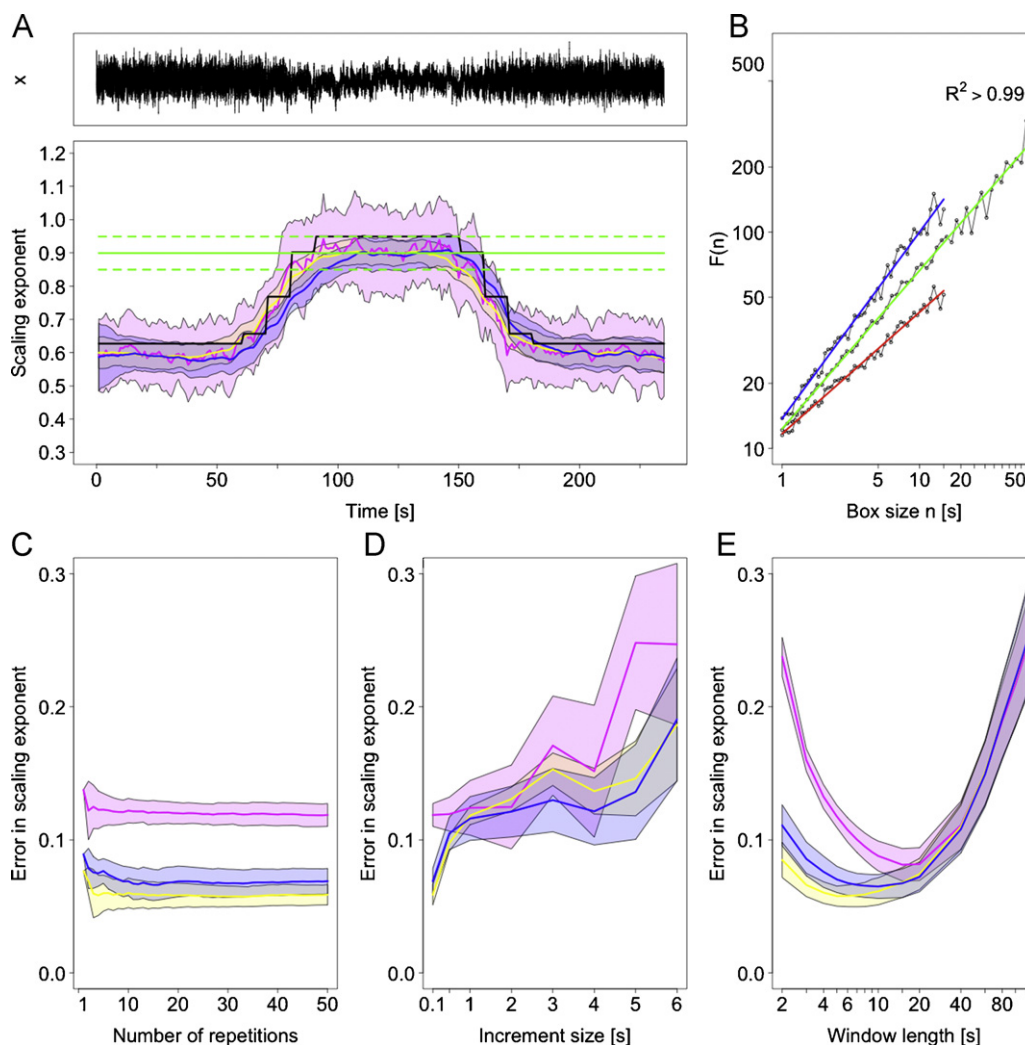


**Fig. 1.** Comparison of DFA, mDFA, ATvDFA using synthetic data with time-varying exponent. (A) (Top panel), sample FARIMA(0,d,0) time series with d systematically varying during the record. (Bottom panel), the black line shows the sequence of exponents ( $H = d + 0.5$ ) used to create the synthetic data such as that shown in the top panel. The solid and dotted green lines are the average and standard deviation of the exponents obtained when using DFA over each of the 50 time series. The mean and standard deviations obtained by the different methods over each of the 50 time series are shown by the magenta (mDFA), blue (ATvDFA without smoothing), yellow (ATvDFA with smoothing) lines and shaded areas. (B) Scaling relationship between log detrended fluctuations and log box sizes for the pre (red), post (blue) exponent inflation and whole record (green). (C)–(E) Dependences of the RMS error (RMSE) of mDFA (magenta), ATvDFA without smoothing (blue) and ATvDFA with smoothing (yellow) on the number of time series used to obtain an average estimate (C), the increment between windows (D) and the window length (E). In D and E, all 50 time series were used to estimate the mean and standard deviation of the RMSE. (For interpretation of the references to colour in this figure legend, the reader is referred to the web version of the article.)

the data appears as a multiplicative term in the expected value of the detrended fluctuations. By normalising the variance, the linear regression of the log detrended fluctuations of two segments with an identical exponent over the log box sizes would be expected to have the same intercept. With this simulation, there was no change in exponents within less than 10 s, and the largest single exponent change was 0.13. Fifty 240 s long time series were created at a sampling rate of 256 Hz (typical in EEG recordings). An example of a resulting time-series is shown in Fig. 1A (top panel).

### 2.3. Physiological data

To demonstrate the range of applications of the method, we considered three possible sources of disruptions/perturbations of the scaling exponent: disruption by manipulation of the data, e.g., localised random shuffling, disruption through experimental manipulation and disruption due to fluctuations of spontaneous origin (or, at least, non systematic origin). We describe each case in order.

#### 2.3.1. Disruption of LRTCs by data manipulation

As multiple studies have confirmed the existence of LRTCs in the fluctuations of oscillation amplitude of seizure-free EEG recordings in a number of frequency bands (e.g., Linkenkaer-Hansen et al., 2001; Nikulin and Brismar, 2005), we used data (sampled at 256 Hz) from the CHB-MIT Scalp EEG Database (Shoeb, 2009) available from PhysioNet (Goldberger et al., 2000). To extract the fluctuations of oscillation amplitude, an EEG record (electrode F8-T8, subject CHB01) was band-pass filtered (black line in Fig. 4A) in the alpha rhythm frequency range (8–12 Hz) and its envelope (red line in Fig. 4A) extracted using the Hilbert transform. A 1-min section of the data confirmed to have constant non-trivial scaling exponent ( $>0.7$ ) was then shuffled to destroy its LRTCs and the tracking methods were applied to the envelope of the whole record including the shuffled section.

#### 2.3.2. Disruption of LRTCs through spontaneous fluctuations

We used electrocorticography interictal data (sampled at 200 Hz) recorded at the Great Ormond Street Hospital (London, UK) on an 11-year-old female who was suffering from intractable

epilepsy and was implanted with a  $6 \times 8$  electrode mesh as part of a pre-assessment for surgery. The data were identified by the consultant clinical neuro-physiologist as showing seizure activity in several electrodes over a finite period of time (see Fig. 5F). Data were processed as in Section 2.3.1.

### 2.3.3. Disruption of LRTCs through experimental manipulation

The EMG signals (sampled at 5 kHz) of the first dorsal interosseus (FDI) muscle of a healthy adult male were recorded during two conditions. In the first (condition LL), the subject maintained a steady voluntary contraction at 10% of MVC for a duration of 90 s with visual feedback of the muscle's force output. In the second condition (condition LH), the subject performed a steady contraction at 10% of MVC for 40 s followed by a 10-s ramp force increment (directed by visual cue which was matched by the subject changing force output) ending at 50% of MVC which the subject then maintained for a further 40 s. The data was band-pass filtered between 23 and 31 Hz which corresponded to a peak in the power spectrum of the rectified EMG (Fig. 5A). Its envelope was then extracted using the Hilbert transform.

## 3. Results

### 3.1. Application to synthetic data

We assessed the performance of ATvDFA and its sensitivity to the choice of its free parameters by applying it to the different time series and systematically varying the free parameters that most affect the physiological interpretation of the results. These are as follows:

- 1 The window length over which the detrended fluctuations are estimated provides the temporal resolution and was varied between 2 s (much shorter than the known order of magnitude of the changes in exponent) and 110 s (almost half of the total record).
- 2 The temporal increment between segments used for estimating the exponent. This also influences the temporal resolution and was varied between 0.1 s (1/100th of the smallest window length) and 6 s (i.e., less than 10 s).
- 3 The number of repetitions which makes it possible to obtain smooth estimates and provides confidence intervals on the results. The number of repetitions was varied between 1 and 50.
- 4 The covariance parameter  $Q$  controls the degree of localisation of the state estimate. The same parameter was used for both components of the state vector and it was varied between  $1E-6$  (very tight) and  $1E-4$  (loose).

#### 3.1.1. Comparison of DFA, mDFA and ATvDFA on changing scaling exponent

We applied DFA, mDFA and ATvDFA (with and without Kalman smoothing) to all time series (a sample of which is shown in the top graph of Fig. 1A). The average value of the DFA exponents computed over the entire time series (solid green line in Fig. 1A) was in between the extrema of the exponents used to construct the time series ( $H = 0.6271$  for the first and final segments,  $H = 0.9491$  for the central segment). Importantly, the linear relationship between the log detrended fluctuations and log box size was maintained (green line in panel B, for one time series) showing that for small changes in exponent the standard DFA algorithm does not provide the means, whether through thresholding of the  $R^2$  value or through visual inspection, to detect the violation of the assumption of constancy of the exponent even if when the changes take place over almost half of the record. In contrast, the estimates (averaged over 50 repetitions) from mDFA (solid magenta line), ATvDFA without Kalman

smoothing (solid blue line) and ATvDFA with Kalman smoothing (solid yellow line) all tracked the changes in exponent within the time series and provided an accurate estimate of both pre- and post-inflation baseline exponent values. The fact that the mean estimates from mDFA, ATvDFA without Kalman smoothing and ATvDFA with Kalman smoothing are very close (RMSE between filtering methods and expected values in range [0.042–0.051]; RMSE between filtering methods in range [0.019–0.037]) is in agreement with similar observations by Peña et al. (2009) and is expected by statistical sampling theory. The standard deviations (coloured areas in Fig. 1A), however, reveal a different picture, with very tight intervals ( $0.039 \pm 0.003$  for ATvDFA with smoothing,  $0.049 \pm 0.008$  for ATvDFA without smoothing) for both versions of ATvDFA compared with those of mDFA ( $0.11 \pm 0.015$ ). This indicates that there are large fluctuations in mDFA estimate profiles between repetitions that reduce the confidence levels on those estimates, both when averaged but more specifically when only one repetition is available (e.g., when applying the method to single physiological time series to locate periods in the record where the scaling exponent changes). This difference in variability of the estimation is illustrated in Fig. 2C where individual time series of estimates are provided for the parameter settings used to produce Fig. 1A. It can be seen that the mDFA estimates (magenta line) fluctuate wildly around the average whilst both forms of ATvDFA provide smooth estimates (blue and yellow lines).

We assessed the RMS error between the sequences of mDFA, ATvDFA (with and without Kalman smoothing) estimates and the sequence of exponents used to generate the data against the three parameters that affect the estimation process: the number of repetitions (or trial number), the window length and the increment time (Fig. 1C–E). Irrespective of the number of trials, the ATvDFA method compares favourably with mDFA with a mean RMSE smaller by a factor 2 (Fig. 1C). Only marginal gains in accuracy were obtained when increasing the number of trials, ATvDFA with Kalman smoothing proving particularly stable. The standard deviations for the RMSEs are equally tight for all methods suggesting that the difference in performance is robust. For both versions of the ATvDFA method, there is a straightforward relationship (Fig. 1D) between RMS error and increment size, with smaller increments leading to more accurate exponent estimates. This is expected since small increments provide for more robust estimates of the measurement noise, and an increased likelihood that the exponent be constant between consecutive windows. In contrast, mDFA is shows little sensitivity to the increment for increment values of less than 3. This illustrates the noisy character of such an estimation process. The mean estimates of ATvDFA without Kalman smoothing (blue line) prove robust to the [1–5 s] range of increment size although the standard deviations increase as expected. The relationship between the RMS error and the window length is shown in Fig. 1E. The results illustrate the trade-off between choosing a long-enough window length that LRTCs can be robustly estimated and short-enough that changes in exponents can be detected. Critically, however, both ATvDFA methods provide a wider range of operation with window lengths in the range [3–30 s] resulting in a level of accuracy equal or better than the best accuracy achieved by mDFA (at  $\sim 15$ –20 s). In the scenario presented here, it was found that a window length of 5 s provided the best estimates for both ATvDFA methods. This is half the duration of the shortest periods of constant exponents (10 s).

Fig. 2A and B provide the ratio of RMSE of Kalman filtered estimates over DFA estimates, and Kalman filtered estimates with smoothing over DFA estimates respectively, over the fluctuating exponent time series. They illustrate the sensitivity of the method to the choice of covariance in relation to the window length, with tighter covariances required for longer window lengths due to potentially more noisy measurements. However, our results (with

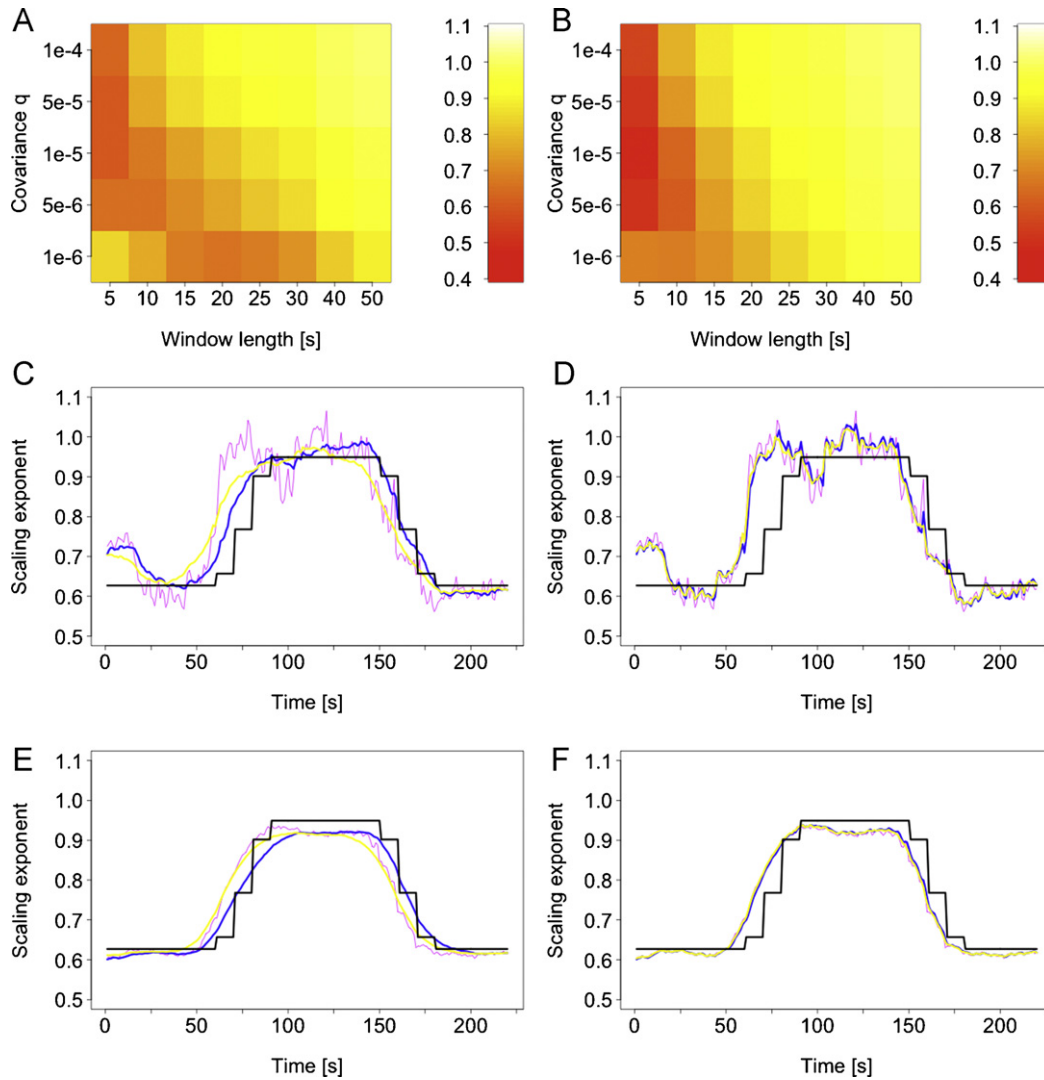


**Fig. 2.** Dependence on choice of covariance parameter. (A) Ratio of RMSE for ATvDFA without smoothing to RSME for mDFA for window lengths in [5–50 s] and covariance parameter  $q$  in [0.000001–0.0001 s]. Darker regions denote parameter settings where ATvDFA without smoothing outperformed mDFA. (B) Same as A for ATvDFA with smoothing. (C) Time series of estimates obtained by mDFA (magenta), ATvDFA without smoothing (blue), ATvDFA with smoothing (yellow) for a single time series constructed as per the series of exponents given by the black line (as in Fig. 1) when the covariance parameter  $q$  and the window length are chosen to minimise the ratio of RMSE in panel B (window length = 5 s, covariance parameter  $q = 1e-5$  s). (D) Time series of estimates obtained when maximising the ratio of RMSE in panel B (window length = 50 s, covariance parameter  $q = 1e-4$  s). (E) and (F) Average of the estimates over 50 time series for parameter settings corresponding to (C) and (D), respectively. (For interpretation of the references to colour in this figure legend, the reader is referred to the web version of the article.)

ratios < 1) demonstrate that the Kalman-based methods always outperform mDFA irrespective of the choice of those parameters. Panels C and D provide individual time series of estimates for all 3 methods for the optimal covariance setting (panel C) and the worse covariance setting (panel D). With an overly loose covariance parameter, the ATvDFA estimates become identical to those of mDFA. Panels E and F provide the same information when averaged over 50 such trials. As shown by Fig. 1A, the mean estimates are very similar between methods irrespective of the choice of the covariance parameters.

### 3.1.2. Comparison of DFA, mDFA and ATvDFA on constant scaling exponent

To further our comparison of the benefit of ATvDFA over mDFA, we applied the methods to long (16,384 s at 256 Hz) time series of known constant exponents (0.6, 0.75 and 0.95), 10 s of which are shown in the three graphs of Fig. 3A. The resulting time-series of exponents are shown in Fig. 3B and compared to the theoretical exponent (black line), and exponent measured by applying DFA over the whole record (red line). Confirming our results with fluctuating exponents, both forms of ATvDFA estimates show the smallest

bias with tight standard deviations. This result did not depend on the choice of exponent as evidenced by histograms of the estimates for the 3 chosen values of exponents (Fig. 3C–E). The sensitivity of the different methods to the choice of window length was assessed by computing the mean and standard deviation of the estimates with window lengths in the range 2–150 s. As expected there is a straightforward relationship between window length and accuracy of the estimates for all techniques, with true values recovered for the longest window lengths shown. The erratic nature of the estimation process of mDFA is clearly illustrated by large standard deviations. The standard deviations converge to those of ATvDFA and ATvDFA with smoothing at window lengths greater than 40 s, confirming that mDFA would be of very limited applicability if spontaneous or induced changes in exponents occurred over short periods.

## 3.2. Application to physiological data

### 3.2.1. Application to surface seizure-free EEG data

DFA, mDFA and ATvDFA (window length of 30 s, increment of 1 s, single trial) were applied to the fluctuations of amplitude in the alpha (8–12 Hz) band of 2.5 min of seizure-free EEG data. A single

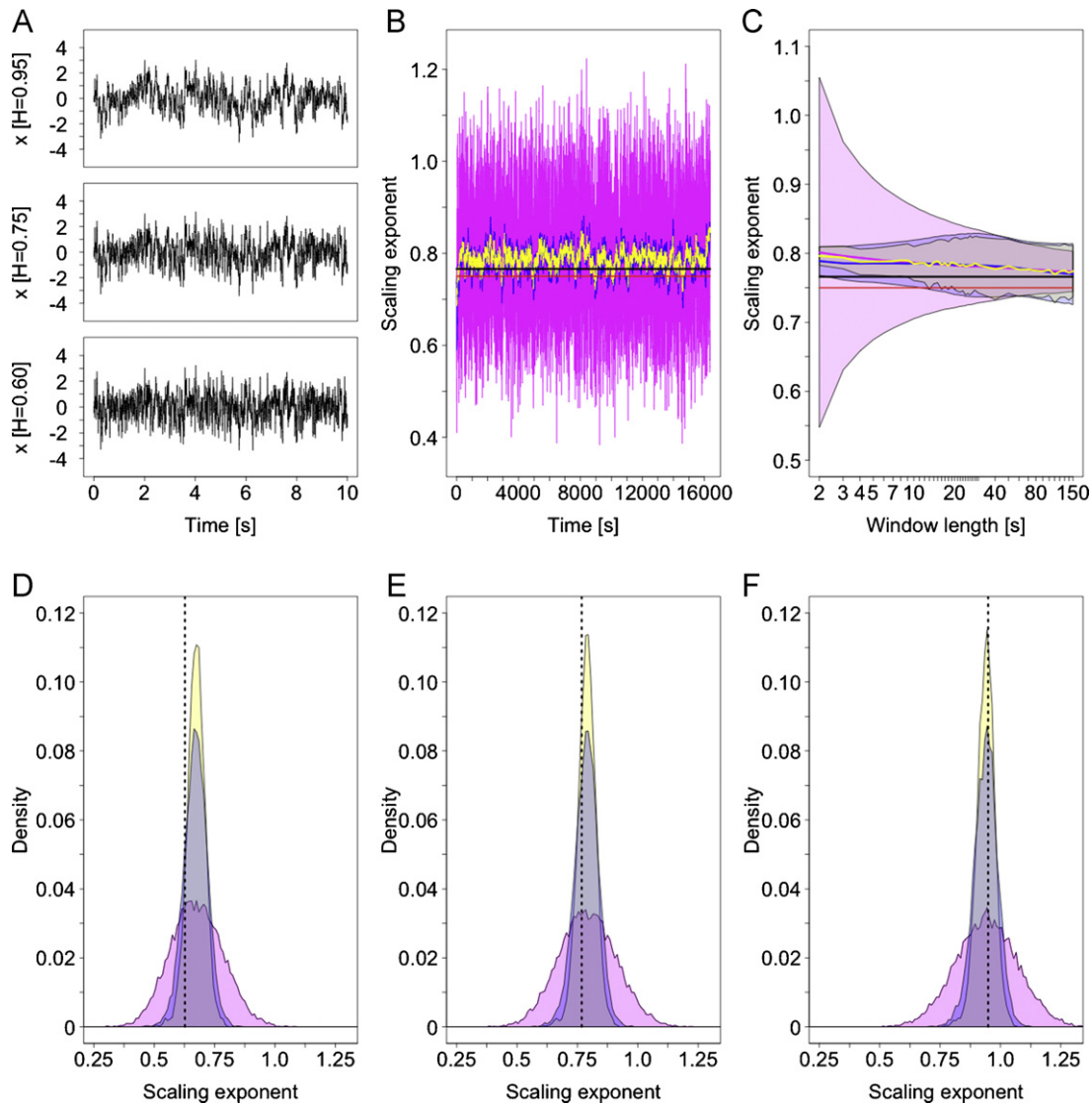


**Fig. 3.** Comparison of DFA, mDFA, ATvDFA using synthetic data with constant exponent. (A) Three short 10 s extracts of FARIMA(0,d,0) processes with  $d=H - 0.5$  taking value 0.45 (top), 0.25 (middle), 0.1 (bottom). (B) Time series of exponents obtained by mDFA (magenta), ATvDFA without smoothing (blue), ATvDFA with smoothing (yellow) on a time series with known fixed exponent 0.75 (measured DFA exponent shown by the black line) when using a window length of 5 s. (C) Relationship of mean and standard deviation of the exponent obtained by mDFA (magenta), ATvDFA without smoothing (blue), ATvDFA with smoothing (yellow) when the window length is taken in the range [2–150 s]. The shaded areas represent the standard deviations of the estimates. The red line denotes the theoretical exponent. The black line denotes the mean exponent obtained by DFA over the whole time series. (D)–(F) Histograms of the estimates obtained by each method for the time series of known exponent 0.6 (D), 0.75 (E) and 0.95 (F). (For interpretation of the references to colour in this figure legend, the reader is referred to the web version of the article.)

DFA exponent of 0.63 (dotted blue line in Fig. 4C) was obtained by application of DFA over the whole record, consistent with published values for this type of data (Nikulin and Brismar, 2005). As in the synthetic data, the linear relationship between the log detrended fluctuations and log box sizes was maintained (blue line in Fig. 4B) therefore providing no indirect indication that there may be a change in exponent. In contrast, the application of mDFA resulted in wildly fluctuating estimates (in range of [0.53–0.96]) consistent with previous observations of the important statistical variation of such an estimation process. More critically, both ATvDFA without smoothing (solid blue line) and ATvDFA with smoothing (yellow line) revealed a series of exponents that slowly fluctuate in time with ranges of [0.70–0.79] and [0.72–0.77] respectively. A section of the EEG (grey rectangle in Fig. 4D) was then shuffled and DFA, mDFA and ATvDFA re-applied. The DFA exponent computed over the whole record showed an unexpected increase (dotted black line in Fig. 4D). Based on the  $R^2$  value ( $>0.98$ ), one would conclude that the linear scaling between log detrended fluctuations and log box

sizes was maintained (red line in Fig. 4B), however, close inspection reveals a cross-over behaviour with fluctuations for box sizes less than 10 s showing an exponent similar to that of the intact record, and the fluctuations for box sizes greater than 10 s showing a steeper slope with more variance at the largest box sizes. For data windows in which the scaling exponent is constant (intact data from 0 to 54 s, shuffled data from 69 s to 114 s, and intact data from 129 s to end of record), mDFA returns noisy estimates around the true value, as in the intact case. For windows that contain data with different exponents (dark grey areas in Fig. 4D), however, mDFA returns spuriously high estimates due to loss of scaling. In contrast, both forms of ATvDFA provide meaningful estimates with a smooth transient between the two expected values.

### 3.2.2. Application to electrocorticography EEG data

DFA, mDFA and ATvDFA (window length of 15 s, increment of 1 s, single trial) were applied to the fluctuations of amplitude in the alpha (8–12 Hz) band of ~16 min of electrocorticography EEG

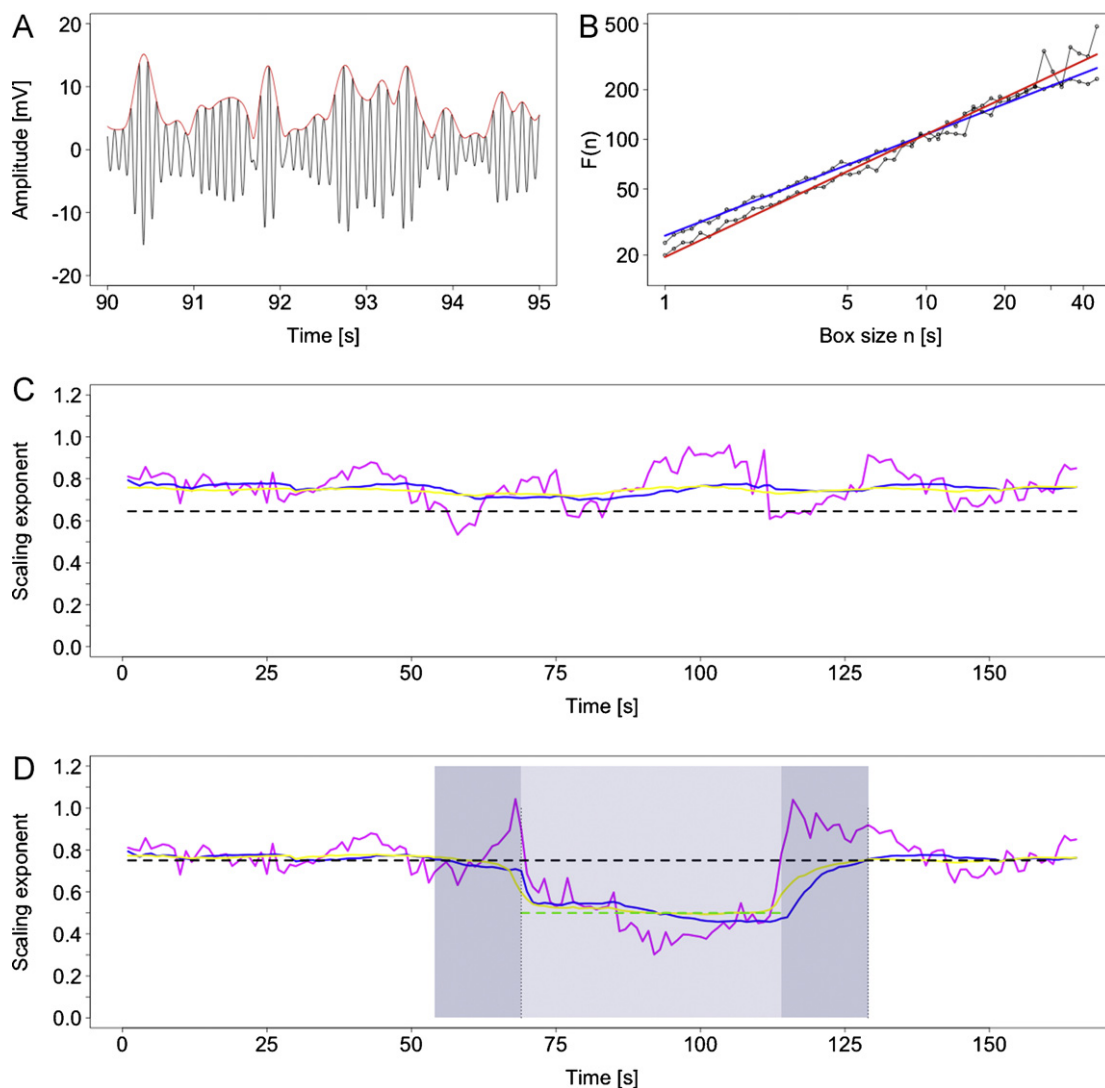


**Fig. 4.** Comparison of DFA, mDFA, ATvDFA using EEG data. (A) Bandpassed EEG (8–13 Hz) with fluctuations of oscillation amplitude (red line). (B) DFA log–log plot of detrended fluctuations versus box sizes for intact (blue) and shuffled (red) EEG records. (C) Exponents obtained by mDFA (magenta), ATvDFA without smoothing (blue), ATvDFA with smoothing (yellow) for the intact record. The dashed black line denotes the exponent obtained by DFA over the whole record. (D) Exponents obtained by mDFA (magenta), ATvDFA without smoothing (blue), ATvDFA with smoothing (yellow) for the partially shuffled (grey area in range 69–129 s) record. The dark grey areas denote time ranges for which the estimates were obtained over windows that included segments of different exponents (intact and shuffled). The green dotted line shows the theoretically expected 0.5 exponent for shuffled data, the black line shows the DFA exponent for the whole record. (For interpretation of the references to colour in this figure legend, the reader is referred to the web version of the article.)

data (2 out of 48 electrodes, G13 in blue and G40 in red in Fig. 5F). Application of DFA over both records yielded values of  $\sim 0.62$  for G13 and  $\sim 0.80$  for G40. The linear relationship between the log detrended fluctuations and log box sizes was maintained for both electrodes (blue and red lines in Fig. 5B) with  $R^2$  values ( $>0.99$  in both instances) providing no indication that there may be a change in exponent during the record. Again, the application of mDFA (magenta line in Fig. 5C and D) resulted in wildly fluctuating estimates (ranges of [0.60–1.06] for G13 and [0.47–1.23] for G40) such that it would not be possible to detect any differences between the two time series with any statistical significance. In contrast, the use of ATvDFA with smoothing revealed a key difference between the sequences of exponents for both electrodes. Whilst the estimates from ATvDFA with smoothing (yellow line in Fig. 5C and D) remain constant over most of the record, electrode G40 (Fig. 5D) shows a localised deviation (decrease in exponent) of more than 2 standard deviations over the period [300–325 s]. Interestingly, this data segment contains an electrographic seizure (see Fig. 5F). Fig. 5E, which shows normalised exponents for G13 (blue line) and

G40 (red line) over that period, reveals that whilst both electrodes show a reduction in exponent, only G40 passes the 2 standard deviations threshold. This is consistent with the degree of involvement of the respective electrodes in that seizure (see Fig. 5F).

### 3.2.3. Application to EMG data for FDI muscle in a simple motor task

DFA, mDFA and ATvDFA (window length of 20 s, increment of 1 s, 2 trials) were applied to the fluctuations of amplitude in the beta (27–31 Hz) band of two repetitions of the two conditions (LL and LH, see Section 2). Application of DFA over both records yielded values of  $\sim 0.57$  for both conditions, with a linear relationship between the log detrended fluctuations and log box sizes maintained in both instances (blue and red lines in Fig. 6B,  $R^2$  values of  $\sim 0.99$  in both conditions). Application of mDFA and ATvDFA with/without smoothing to the LL condition data (dashed magenta, blue and yellow lines in Fig. 6C) shows qualitatively similar results to previous examples with mDFA providing noisy estimates and ATvDFA with and without smoothing yielding similar and near constant

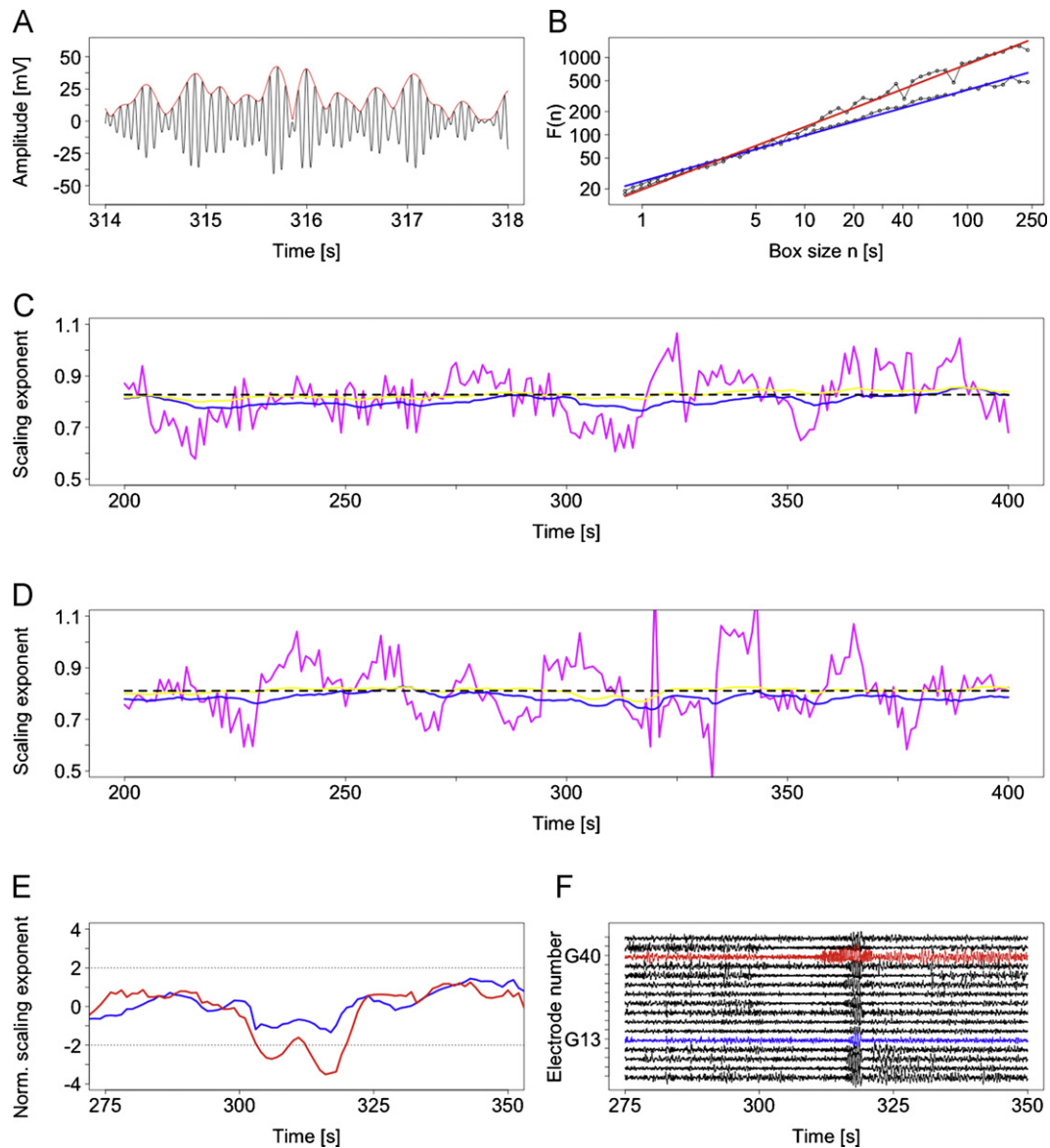


**Fig. 5.** Comparison of DFA, mDFA and ATvDFA using electrocorticography data. (A) Bandpassed electrocorticography signal (8–12 Hz) with fluctuations of oscillation amplitude (red line). (B) DFA log–log plot of detrended fluctuations versus box sizes for electrodes G13 (blue) and G40 (red) in a grid of 48. (C) and (D) Exponents obtained by mDFA (magenta), ATvDFA without smoothing (blue), ATvDFA with smoothing (yellow) for records G13 and G40 respectively. The dashed black line denotes the exponents obtained by DFA over the whole records. (E) Normalised scaling exponents obtained by ATvDFA with smoothing for G13 (blue) and G40 (red) in the period [275–350 s]. The dotted black lines denote 2 standard deviations. (F) Traces for all 48 electrodes over the same period, with G13 and G40 shown in blue and red respectively. An electrographic seizure occurs in the interval [300–325 s]. (For interpretation of the references to colour in this figure legend, the reader is referred to the web version of the article.)

estimates in the range [0.57–0.61] for ATvDFA without smoothing (blue) and [0.58–0.61] for ATvDFA with smoothing. In contrast, the exponents produced by all three estimators is shown to fluctuate distinctly in the LH condition (solid magenta, blue and yellow lines in Fig. 6C). Importantly, these fluctuations are localised to the ramp period (40–50 s, dark grey area) and windows which contain data with different exponents (light grey areas). In the high-force regime, the exponents return to the values observed in the low-force regime, therefore excluding the possibility that the increase in exponent would correlate with the expected increase in coefficient of variation of the data (Jones et al., 2002). In other words, application of ATvDFA makes it possible to detect a change in the order of the data during the ramp. A full presentation and discussion of this study is beyond the scope of this paper and will be given elsewhere.

#### 4. Discussion

The importance of the proposed ATvDFA method is that it provides a robust estimate of the exponent and changes in the magnitude of the exponent during a time series. From the simulations presented here the temporal resolution of the estimate can be as little as a few seconds. Robust estimates of the DFA exponent (RMS error <0.1) can be obtained from a single time series without averaging (see Fig. 3). The difference between ATvDFA with and without smoothing and mDFA is well illustrated in Fig. 3B in which the synthetic FARIMA data was constructed to have a constant exponent of 0.75. The exponent recovered from the entire time series is 0.76, the ATvDFA methods recover exponent values that fluctuate around 0.77 within a narrow range. In contrast the mDFA estimates fluctuate between 0.4 and 1.2, i.e. across an exponent range that

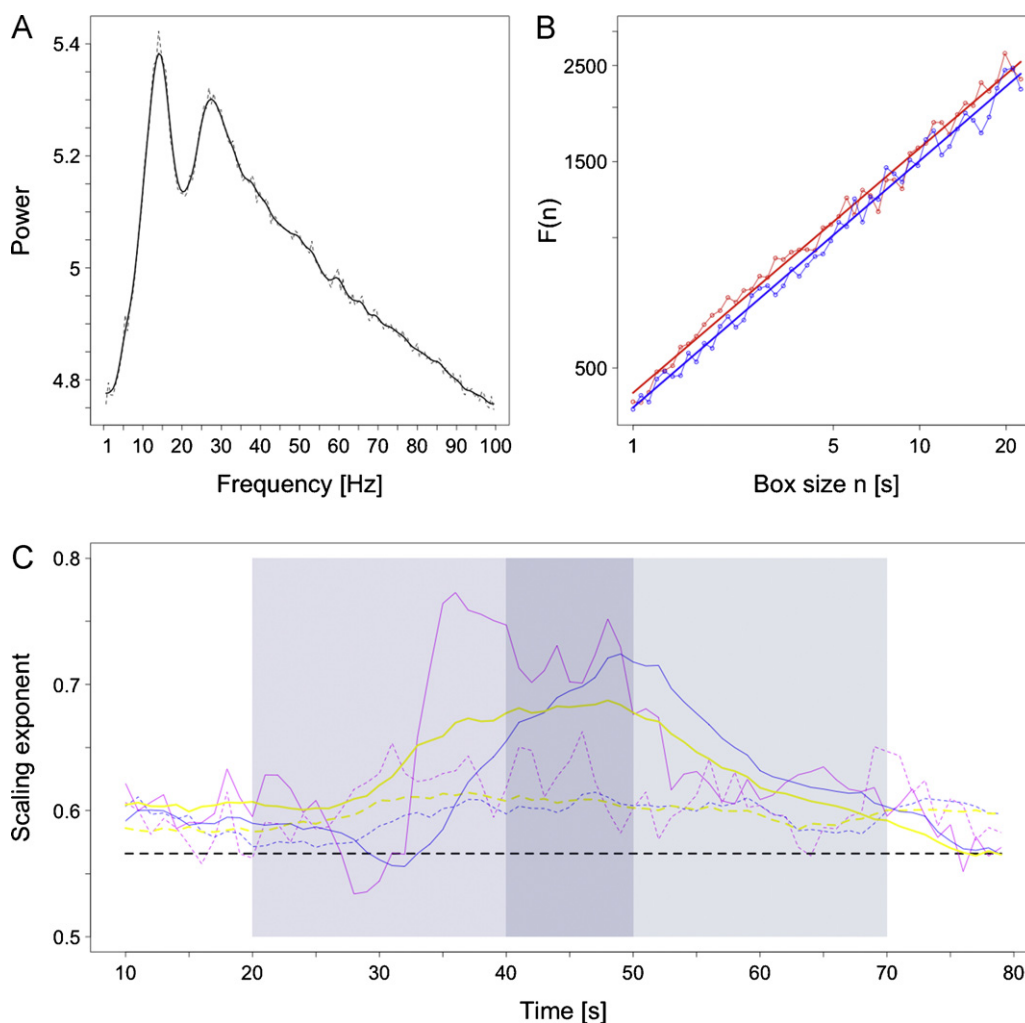


**Fig. 6.** Comparison of DFA, mDFA and ATvDFA using EMG data. (A) Power spectrum for the EMG data of the FDI muscle during the motor task, averaged over all trials. The dotted line shows the raw spectrum. The solid line shows the fitted spectrum used to extract the location of the peaks. The data show a peak in the beta band at 27 Hz. (B) DFA log-log plot of detrended fluctuations versus box sizes for one trial of condition LL (blue) and one trial of condition LH (red). (C) Exponents obtained by mDFA (magenta), ATvDFA without smoothing (blue), ATvDFA with smoothing (yellow) for the LL condition (dotted lines) and for the LH condition (solid lines). The black line denotes the exponents obtained by DFA over the whole record of each of the two conditions (0.57 for both conditions). The light grey areas [20–40 s, 50–70 s] correspond to data windows containing data with changing exponents. (For interpretation of the references to colour in this figure legend, the reader is referred to the web version of the article.)

comprises Gaussian white noise (DFA  $\sim 0.5$ ) and its integration into a Brownian process (DFA  $\sim 1.5$ ). Therefore in comparison to ATvDFA mDFA provides an unreliable method for estimating the exponent value of a single time series and is unsuited for estimating either the moment-to-moment fluctuations within a constant experimental/recording paradigm or experimentally induced exponent changes. As explored in the Results section, a limitation of the ATvDFA method lies with the choice of the parameters of the process noise covariance matrix  $Q$ . As pointed out in Section 2, the choice of these parameters implements a trade-off between temporal localisation of the estimate and consistency. Application of DFA to short data segments will lead to large variations in the log detrended fluctuations from one segment to the other as evidenced by the application of mDFA on data of known exponents (see Fig. 3). Tight covariance parameters result in the filter being too sensitive to these variations leading to inconsistent values, albeit with good temporal resolution. By relaxing the covariance parameters, the filter can show increased consistency. Conversely, for long data segments, where DFA will be more oblivious to loss of scaling due to a locally changing exponent, the use of tight covariance parameters improves temporal localisation. This trade-off is illustrated by

Fig. 2C and D. It should be noted that this trade-off is mostly relevant to the use of ATvDFA in single-trial data. For multi-trial data, the method is relatively insensitive to the choice of the  $Q$  parameters (see Fig. 2E and F) as expected by statistical sampling theory. Furthermore, it should be noted that ATvDFA with smoothing is less sensitive to the exact selection of the  $Q$  parameters. A comparison between Fig. 2A and B shows that the domain of parameters over which the method produces optimal performance displays less structure in the relationship between  $Q$  parameters and window length. This is because the smoothing filter provides consistency when the covariance parameters are tightened to improve localisation. We suggest that in experimental situations where one might anticipate rapid and frequent changes in exponents values, ATvDFA with smoothing should be used with a small window length and  $Q$  parameters selected using Fig. 2B as a guide.

A number of investigators have applied detrended fluctuation analysis to assess the presence of long-range temporal correlations through an estimate of the Hurst exponent in EEG and MEG time series (Linkenkaer-Hansen et al., 2001, 2004, 2004; Nikulin and Brismar, 2005; Berthouze et al., 2010). These studies have been carried out under the implicit assumption that, providing

the experimental and recording conditions are kept constant, any exponent value recovered from DFA relates to an overall brain state present during the entire length of the time series record. Our method suggests that, even in the absence of experimental manipulations, the validity of such an assumption should be ascertained, as there may be spontaneous changes in the determinancy of the signal which could be detected as fluctuations in the magnitude of the estimated exponent on a fine enough time scale. Such spontaneous changes in brain state characterised by fluctuations in intrareal BOLD signal correlations are well described in the literature on the resting state fMRI (e.g., Ko et al., 2011). Resting state fluctuations are also observed in EEG gamma rhythm power (Deco et al., 2011). The ATvDFA methodology described here provides investigators with the means to assess the presence of spontaneous changes in the scaling exponents that characterize LRTCs within a neurophysiological time series and may thus open new avenues for analysing and understanding the brain resting state.

EEG and MEG studies of normal human development and neuropsychiatric disease states have detected consistent differences in exponent magnitude between different groups with a tendency for LRTCs to increase with brain maturation (Smit et al., 2011) and decrease with neurological disease states (e.g. autism, depression, schizophrenia and Alzheimer's disease (Lai et al., 2010; Linkenkaer-Hansen et al., 2005; Montez et al., 2009)). However, little is known about the functional significance of the differences in exponent magnitude (Smit et al., 2011). It has been speculated that the magnitude of the exponent reflects the temporal integration span of brain activity and the information content of brain activity, with lower exponent values representing brain states that are noisy yet highly flexible and high exponent values representing brain states that are more stable, more correlated yet less flexible (Smit et al., 2011). The development of a robust measure of exponent magnitude changes on a short enough time scale to be amenable to experimental manipulation will allow the functional significance of exponent magnitude to be explored empirically. ATvDFA provides a new avenue for studying experimental paradigms in which a task or stimulus might induce changes in the temporal order of the brain activity. This will enable researchers to devise experiments in which the functional significance of exponent value can be established.

## Acknowledgements

The authors would like to thank Dr Stewart Boyd for providing the electrocorticography data, and Drs Tue Petersen and Marco Davare for recording the motor data. They are also grateful to the constructive and helpful comments from two anonymous referees. SF was funded by UCLH CBRC (University College London Hospitals Comprehensive Biomedical Research Centre).

## References

- Alvarez-Ramirez J, Alvarez J, Rodriguez E, Fernandez-Anaya G. Time-varying Hurst exponent for US stock markets. *Physica A* 2008;387(2):6159–69.
- Bardet J. Asymptotic properties of the detrended fluctuation analysis of long-range-dependent processes. *IEEE Trans Inf Theory* 2008;54(5):2041–52.
- Benayoun M, Cowan JD, van Drongelen W, Wallace E. Avalanches in a stochastic model of spiking neurons. *PLoS Comput Biol* 2010;6(7):e1000846.
- Berthouze L, James LM, Farmer SF. Human EEG shows long-range temporal correlations of oscillation amplitude in Theta, Alpha and Beta bands across a wide age range. *Clin Neurophysiol* 2010;121(8):1187–97.
- Box G, Jenkins G. *Time series: forecasting and control*. San Francisco: Holden-day; 1976.
- Brittain JS, Catton C, Conway BA, Nielsen JB, Jenkinson N, Halliday DM. Optimal spectral tracking-with application to speed dependent neural modulation of tibialis anterior during human treadmill walking. *J Neurosci Methods* 2009;177(2):334–47.
- Brown R, Hwang P. *Introduction to random signals and applied Kalman filtering*. New York: John Wiley & Sons; 1997.
- Buckley CL, Nowotny T. Multiscale model of an inhibitory network shows optimal properties near bifurcation. *Phys Rev Lett* 2011;106(23):238109.
- Chen Z, Ivanov P, Hu K, Stanley H. Effect of nonstationarities on detrended fluctuation analysis. *Phys Rev E* 2002;65(4):041107.
- Chialvo DR. Emergent complex neural dynamics. *Nat Phys* 2010;6(1):744–50.
- Crevecoeur F, Bollens B, Detrembleur C, Lejeune TM. Towards a “gold-standard” approach to address the presence of long-range auto-correlation in physiological time series. *J Neurosci Methods* 2010;192(1):163–72.
- Deco G, Jirsa VK, McIntosh AR. Emerging concepts for the dynamical organization of resting-state activity in the brain. *Nat Rev Neurosci* 2011;12(1):43–56.
- Goldberger AL, Amaral LAN, Glass L, Hausdorff JM, Ivanov PC, Mark RG, et al. *PhysioBank, PhysioToolkit, and PhysioNet: components of a new research resource for complex physiologic signals*. *Circulation* 2000;101(23):e215–20.
- Hartikainen J, Solin A, Särkkä S. EKF/UKF Toolbox for Matlab V1.3. <http://becs.aalto.fi/en/research/bayes/ekfukf/>; [last accessed 06.12.11].
- Hartley C, Berthouze L, Mathieson SR, Boylan GB, Rennie JM, Marlow N, et al. Long-range temporal correlations in the EEG bursts of human preterm babies. *PLoS One* 2012;7(2):e31543.
- Hosking J. Fractional differencing. *Biometrika* 1981;68(1):165–76.
- Hu K, Ivanov PC, Chen Z, Carpena P, Stanley HE. Effect of trends on detrended fluctuation analysis. *Phys Rev E Stat Nonlin Soft Matter Phys* 2001;64(1 Pt 1):011114.
- Jones KE, Hamilton AF, Wolpert DM. Sources of signal-dependent noise during isometric force production. *J Neurophysiol* 2002;88(3):1533–44.
- Kello CT, Brown GDA, Ferrer-I-Cancho R, Holden JG, Linkenkaer-Hansen K, Rhodes T, et al. Scaling laws in cognitive sciences. *Trends Cogn Sci* 2010;14(5):223–32.
- Kinouchi O, Copelli M. Optimal dynamical range of excitable networks at criticality. *Nat Phys* 2006;2(5):348–51.
- Ko AL, Darvas F, Poliakov A, Ojemann J, Sorensen LB. Quasi-periodic fluctuations in default mode network electrophysiology. *J Neurosci* 2011;31(32):11728–32.
- Lai MC, Lombardo MV, Chakrabarti B, Sadek SA, Pasco G, Wheelwright SJ, et al. MRC AIMS Consortium, Suckling J. A shift to randomness of brain oscillations in people with autism. *Biol Psychiatry* 2010;68(12):1092–9.
- Linkenkaer-Hansen K, Monto S, Rytsälä H, Suominen K, Isometsä E, Kähkönen S. Breakdown of long-range temporal correlations in theta oscillations in patients with major depressive disorder. *J Neurosci* 2005;25(44):10131–7.
- Linkenkaer-Hansen K, Nikouline VV, Palva JM, Ilmoniemi RJ. Long-range temporal correlations and scaling behavior in human brain oscillations. *J Neurosci* 2001;21(4):1370–7.
- Linkenkaer-Hansen K, Nikulin VV, Palva JM, Kaila K, Ilmoniemi RJ. Stimulus-induced change in long-range temporal correlations and scaling behaviour of sensorimotor oscillations. *Eur J Neurosci* 2004;19(1):203–11.
- Magnasco MO, Piro O, Cecchi GA. Self-tuned critical anti-Hebbian networks. *Phys Rev Lett* 2009;102(25):258102.
- McSharry P. DFA Matlab code. <http://www.eng.ox.ac.uk/samp/software/cardiodynamics/dfa.m>; [last accessed 07.10.09].
- Meisel C, Gross T. Adaptive self-organization in a realistic neural network model. *Phys Rev E Stat Nonlin Soft Matter Phys* 2009;80(6 Pt 1):061917.
- Montez T, Poil SS, Jones BF, Manshanden I, Verbunt JPA, van Dijk BW, et al. Altered temporal correlations in parietal alpha and prefrontal theta oscillations in early-stage Alzheimer disease. *Proc Natl Acad Sci USA* 2009;106(5):1614–9.
- Nikulin VV, Brismar T. Long-range temporal correlations in electroencephalographic oscillations: Relation to topography, frequency band, age and gender. *Neuroscience* 2005;130(2):549–58.
- Peña MA, Echeverría JC, Garcá a MT, González-Camarena R. Applying fractal analysis to short sets of heart rate variability data. *Med Biol Eng Comput* 2009;47(7):709–17.
- Peng CK, Buldyrev SV, Havlin S, Simons M, Stanley HE, Goldberger AL. Mosaic organization of DNA nucleotides. *Phys Rev E Stat Phys Plasmas Fluids Relat Interdiscip Topics* 1994;49(2):1685–9.
- Serinaldi F. Use and misuse of some Hurst parameter estimators applied to stationary and non-stationary financial time series. *Physica A* 2010;389(1):2770–81.
- Shew WL, Yang H, Petermann T, Roy R, Plenz D. Neuronal avalanches imply maximum dynamic range in cortical networks at criticality. *J Neurosci* 2009;29(49):15595–600.
- Shoeb A. Application of machine learning to epileptic seizure onset detection and treatment. Ph.D. thesis, Massachusetts Institute of Technology; 2009.
- Smit DJA, de Geus EJC, van de Nieuwenhuijzen ME, van Beijsterveldt CEM, van Baal GCM, Mansvelder HD, et al. Scale-free modulation of resting-state neuronal oscillations reflects prolonged brain maturation in humans. *J Neurosci* 2011;31(37):13128–36.
- Taqqu M, Teverovsky V. Estimators for long range dependence: an empirical study. *Fractals* 1995;3(4):785–98.
- Touboul J, Destexhe A. Can power-law scaling and neuronal avalanches arise from stochastic dynamics? *PLoS One* 2010;5(2):e8982.
- Wagenmakers EJ, Farrell S, Ratcliff R. Estimation and interpretation of  $1/f^{\alpha}$  noise in human cognition. *Psychon Bull Rev* 2004;11(4):579–615.
- Yue J, Shang P, Dong K. Time-dependent Hurst exponent in traffic time series. In: IEEE international conference on information theory and information security (ICITIS); 2010. p. 744–6.